

# Design of Tendon-Driven Robotic Fingers: Modeling and Control Issues

G. Borghesan, G. Palli and C. Melchiorri

*DEIS - Dipartimento di Elettronica, Informatica e Sistemistica  
Università di Bologna  
Viale Risorgimento 2, 40136 Bologna, Italy  
{gianni.borghesan, gianluca.palli, claudio.melchiorri}@unibo.it*

**Abstract**—This paper reports the modeling activities related to the development of an innovative tendon-driven robotic finger, designed as the fundamental element of a new biologically-inspired artificial hand. The finger is realized in plastic material by means of 3D-printing, a production process that allows a remarkable simplification of the mechanical design. Through 3D-printing, we were able to easily implement solutions that could be very difficult, if not impossible, to obtain with conventional manufacturing.

A detailed simulation model of the robotic finger has been developed with the aim not only of designing and testing suitable control strategies for the finger, but also of investigating the benefits and the flaws of particular design solutions. As a matter of fact, this approach to design and realization of robotic fingers, that fulfills the requirements in terms of compactness, integration and simplified assembly, has a significant drawback in frictional phenomena on both tendons and joints. For this reason, an adapted LuGre friction model is proposed in order to simulate and study the finger behavior.

**Index Terms**—Robotic Hands, Tendon Transmission, Friction Modeling, Nonlinear Systems.

## I. INTRODUCTION

The design and realization of multifingered hands is an important research topic in the robotic community, and has been widely studied since the mid 80's. While the initial purpose in developing such devices was to overcome the lack of flexibility of traditional end-effectors [1], nowadays one of the driving issues is to mimic the human's hand capabilities, and more in general to improve their anthropomorphism level. Anthropomorphism is sought for a number of reason and at various levels, from the possibility of imitating how humans approach fine manipulation problems, where dexterity is necessary, to the employment as prosthetic devices, where aesthetics is an important issue.

Our goal is to obtain a dexterous device, resembling the human hand on many constructive aspects, e.g. the mechanical and kinematic structure, the dimensions and the workspace, the compliance of the driving system (muscles and tendons), the compliance and shape of finger pads, the sensitive capabilities, etc. [2]–[4].

This research has been partially funded by the EC Seventh Framework Programme (FP7) under grant agreement no. 216239 as part of the IP DEXMART (DEXterous and autonomous dual-arm/hand robotic manipulation with sMART sensory-motor skills: A bridge from natural to artificial cognition).

Following this “bio-inspired” rationale, a number of choices have been made in the mechanical design, and in particular tendons are used as media to transmit forces from the actuators to the fingers' joints. As reported in [5], where a review of robotic hands is presented, many under-actuated devices have been developed, i.e. robotic hands where kinematic couplings or compliant elements are introduced to correlate the movements of some fingers/phalanges. This solution reduces the number of actuators, but also limits the hands DOF and, in some extent, also their manipulation capabilities. In particular, in [6] the use of a non-actuated (or passive) tendon that couples the medial and distal joints of the robotic fingers has been inspired by the tendon network configuration of the human hand.

Moreover, the new robotic finger under development (that is described in [7]) has been designed following a mechatronic approach, so that all the components, as the mechanical structure, the electronics, the sensors and the actuation system are customized and integrated together. This approach is pursued as a profitable way to obtain higher capabilities, as reported by different authors, see e.g. [8]. This work is centered on the finger modeling, with a particular emphasis on some aspects that we regards as critical (tendon and joint friction). The benefit of the model knowledge is dual, as it will be used in future finger designs, as well as it is necessary in the development of significant control strategies. As secondary contribution, in this work are reported some control strategies (control of tendon forces and joint angles) and some data gathered by simulation.

## II. DESCRIPTION OF THE ROBOTIC FINGER

A tendon-actuated finger is considered in this paper. A coupling tendon (also referred in the text as “passive tendon”) is introduced in order to impose a kinematic coupling between the movements of the last two joints. The mechanical structure of the finger is realized by means of a 3D-printing process, and is entirely composed by *Fullcure®720*, i.e. no other mechanical parts have been used for the finger implementation apart from sensors and electronics; the selection of this particular material has been made because of the limited choice available for the production process. The great flexibility of the adopted construction method allows the placement of finger joints and tendon pathways inside the

phalanges structure, with a level of precision and complexity difficult (if not impossible) to obtain by means of conventional manufacturing. An important drawback involved by this method is the presence of friction forces acting both on the joints, due to the relative movement of surfaces, and on the tendons, due to the sliding of tendons along their pathways. Because of the relevance of these phenomena, a significant effort has been dedicated to model them, as reported in Sec. IV-A.

The finger is constituted by a 4-DOF mechanical structure, whose kinematics (considering the finger tip position as endpoint) is described by the Denavit-Hartenberg parameters summarized in Table I.

The finger is actuated by means of four tendons: three agonistic tendons plus one antagonist tendon. An additional non-actuated tendon is used to couple the movements of the last two joints (medial and distal) inside the finger structure. This tendon configuration is known in literature as a “N+1” tendon network configuration [9], since all joints share an antagonist tendon. The tendons are fixed to the phalanges and routed inside the finger through suitable designed canals. The tendon are constituted by FastFlight® cables: a complete analysis on the tendon transmission modeling, control and material selection is reported in [10].

Tendon pathways have been designed so that tendons envelope on curved surfaces with constant radius along the entire joints movement range, leading to a linear relation between tendon and joint displacements.

### III. FINGER KINEMATICS

From the Denavit-Hartenberg parameters of the finger given in Table I, it is straightforward to compute the finger tip position  $p_{\text{eff}}$  with respect to the base reference frame:

$$p_{\text{eff}} = \begin{bmatrix} C_1(a_1 + a_2C_2 + a_3C_{23} + a_4C_{234}) \\ (a_1 + a_2C_2 + a_3C_{23} + a_4C_{234})S_1 \\ a_2S_2 + a_3S_{23} + a_4S_{234} \end{bmatrix} \quad (1)$$

where  $C_{ijz}$  and  $S_{ijz}$  stand for  $\sin(\theta_i + \theta_j + \theta_z)$  and  $\cos(\theta_i + \theta_j + \theta_z)$  respectively. The joint angle ranges are mechanically constrained by stroke limiters:

$$\theta_1 \in [-\pi/18, \pi/18], \quad \theta_{\{2,3,4\}} \in [0, \pi/2] \quad [\text{rad}] \quad (2)$$

Link 0 is the base of the finger (the hand palm) and is considered fixed. The other links are numbered from 1 to 4 (abduction link, proximal, medial and distal phalanx respectively). The tendons are numbered from  $T_1$  to  $T_5$ , as shown in Fig. 1:

$T_1, T_2$ : Tendons 1 and 2 are attached to the link 2 (proximal phalanx) and drive the first two joints.

Link	$d$	$\theta$	$a$ [m]	$\alpha$
1	0	$\theta_1$	$a_1 = 20.2 \cdot 10^{-3}$	$\pi/2$
2	0	$\theta_2$	$a_2 = 45.0 \cdot 10^{-3}$	0
3	0	$\theta_3$	$a_3 = 29.9 \cdot 10^{-3}$	0
4	0	$\theta_4$	$a_4 = 21.8 \cdot 10^{-3}$	0

TABLE I  
DENAVIT-HARTENBERG PARAMETERS OF THE FINGER.

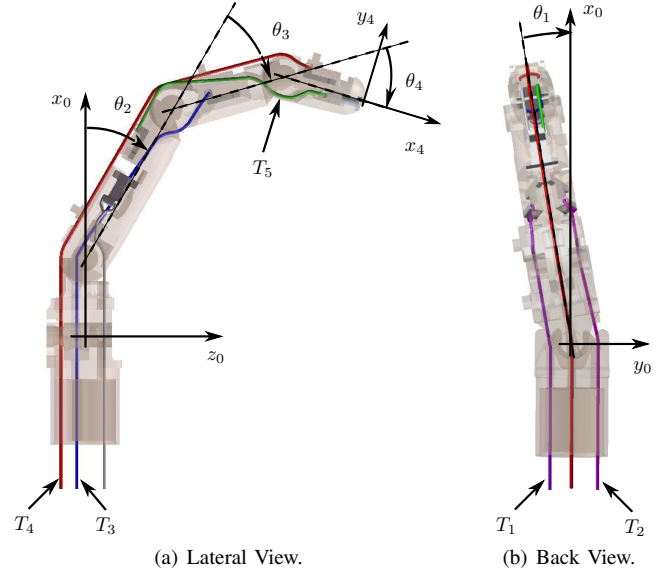


Fig. 1. Tendon configuration and reference angles.

- $T_3$ : Tendon 3 drives the medial joint and is attached to the medial phalanx.
- $T_4$ : Tendon 4 is the antagonist tendon and is attached to the distal phalanx.
- $T_5$ : Tendon 5 is the passive tendon and connects the proximal with the distal phalanx.

Due to the particular design and neglecting the tendon elasticity, the relation between the joint angles and the tendon displacements  $l = [l_1 \ l_2 \ l_3 \ l_4 \ l_5]^T$  can be considered linear:

$$l = H_c \theta, \quad H_c = \begin{bmatrix} r_{11} & r_{21} & 0 & 0 \\ -r_{11} & r_{21} & 0 & 0 \\ 0 & 0 & r_{33} & 0 \\ 0 & -r_{24} & -r_{34} & -r_{44} \\ 0 & 0 & -r_{35} & r_{45} \end{bmatrix} \quad (3)$$

where  $r_{ij}$  is the radius of the circular surface where the  $i$ -tendon envelops itself, on the  $j$ -joint; it has been already considered in (3) the equalities  $r_{12} = r_{11}$  and  $r_{22} = r_{21}$ . In Tab. II are reported the numerical values of  $r_{ij}$ .

By considering  $l_5 = 0$ , i.e. supposing the tendon  $T_5$  inextensible, the last line of eq. (3) gives the kinematic constraint imposed by the passive tendon:

$$\theta_4 = \frac{r_{35}}{r_{45}} \theta_3 \quad (4)$$

Aiming at reducing the dimension and the weight of the robotic finger, very thin tendons made by polymeric fibers have been chosen. As a consequence, the resulting stiffness

	$r_{11}$	$r_{21}$	$r_{33}$	$r_{24}$	$r_{34}$	$r_{44}$	$r_{35}$	$r_{45}$
radius [mm]	5.7	4.5	5.3	6.2	5.3	4.9	4.9	4.4

TABLE II  
RADI OF THE FINGER CIRCULAR SURFACES.

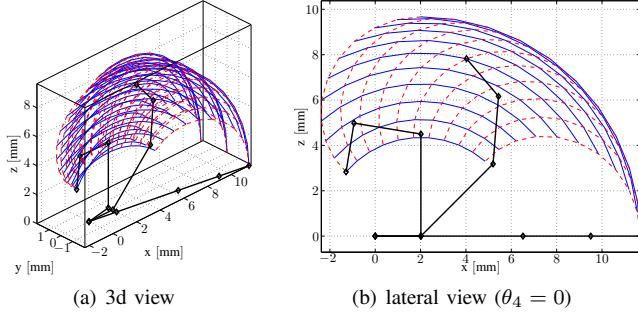


Fig. 2. Finger workspace.

of the transmission system is limited (for the agonist, the antagonist and the passive tendons), and the relation between the movements of the last two joints cannot be longer considered related by a kinematic constraint anymore, but the effect of the force acting on the passive tendon must be considered. If the tendon has a linear elastic coefficient  $K_t$  [10] and friction is negligible, from (3) it is possible to compute the relation between the force  $f_5$  applied to the passive tendon and its elongation  $l_5$ :

$$f_5 = \begin{cases} -K_t l_5 = -K_t(\theta_3 r_{35} - \theta_4 r_{45}) & l_5 > 0, \\ 0 & l_5 \leq 0. \end{cases} \quad (5)$$

Obviously  $l_5 \leq 0$  means that the tendon is slacking: this condition must be avoided by means of a proper control strategy. In Fig. 2 the finger workspace is shown assuming the constrain expressed by eq. (4).

Actuators have been modeled as ideal force generators that impose the force vector  $f^a = [f_1^a \ f_2^a \ f_3^a \ f_4^a]^T$ , since the ultimate selection of the actuation system for the robotic hand under development has not been made yet.

#### IV. FINGER STATIC AND DYNAMIC ANALYSIS

The analysis of tendon forces and joint torques is considered in this section. The relation between the fingertip forces  $F = [F_x \ F_y \ F_z]^T$  and joint torques  $\tau = [\tau_1 \ \tau_2 \ \tau_3 \ \tau_4]^T$  is given by [11]:

$$\tau = J^T F, \quad J = \frac{\partial p_{\text{eff}}(\theta)}{\partial \theta} \quad (6)$$

In the same way, the relation between the tendon tension  $f$  and the joint torques  $\tau$  can be computed as [12]:

$$\tau = H c^T f \quad (7)$$

Since relations (6) and (7) do not take into account the friction acting on both the tendons and the joints, the input force vector  $f$  is defined as

$$f = [f_1 \ f_2 \ f_3 \ f_4 \ f_5]^T \equiv [f_1^a \ f_2^a \ f_3^a \ f_4^a \ f_5]^T \quad (8)$$

where the last element  $f_5$  is given by (5).

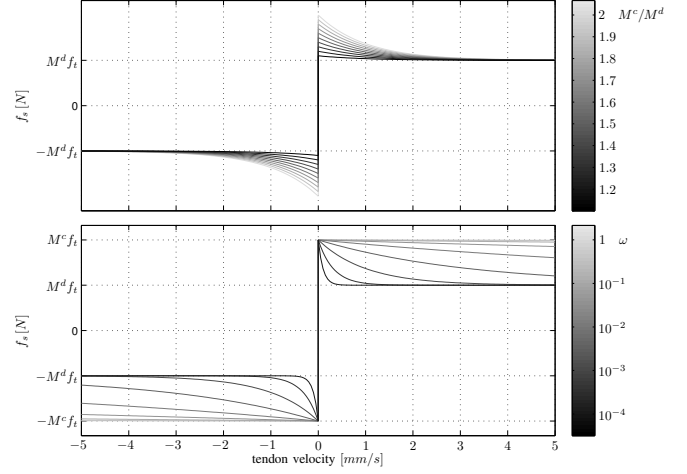


Fig. 3. Friction law for  $F^n = 10N$ : (top) varying  $M^c$ , (bottom) varying  $\omega$ .

#### A. Friction Models

The conventional formulation of the LuGre friction has been specialized for our application, in order to take into account many aspects of the system considered here, like the direction dependent behavior, the dependence of the normal force from the finger configuration and so on. In [13] the different behaviors shown by static and dynamic friction models (Dahl model) in the rendering of the friction phenomena acting on the tendon-based driving system have been evaluated, and the better physical resemblance of the Dahl friction model has been reported. Despite its complexity, the LuGre dynamic friction model has been chosen in this activity to further improve the fitting between simulation and experimental results. In the following a general expression will be given, and then will be described how to specialize it for the two cases. The adopted friction model is described by:

$$\dot{F}^s = \sigma_0 \left( v - \frac{F^s}{F^n M} |v| \right) \quad (9a)$$

$$M = M^d + (M^c - M^d) e^{-\frac{|v|}{\omega}} \quad (9b)$$

$$F^f = F^s + b v \quad (9c)$$

where  $F^f$  is the total friction force,  $F^s$  is the force loss due to stiction,  $F^n$  is the normal force,  $v$  is the velocity, and  $M^d$  is the Coulomb friction coefficient,  $M^c$  is the stiction coefficient and  $\omega$  is the Stribeck velocity. In Fig. 3 the static characteristic of the adopted friction model (i.e. for  $\dot{F}^s = 0$  in (9a)) is shown with respect to the velocity  $v$  for a chosen set of parameters and varying the ratio  $M^c/M^d$  (top) and the Stribeck velocity  $\omega$  (bottom), in order to graphically represent which is the influence of these parameters on the system.

#### B. Tendon Force Analysis

In [13] the friction acting on the tendon has been simulated by means of a lumped spring-mass system and the Dahl dynamic model has been adopted to implement the friction

phenomenon, while in [14] the equivalence between the lumped spring-mass-friction model considered in [13] and a single mass subject to friction (with a suitable choice of the friction parameters) has been shown. In this paper, the tendon behavior has been simulated by means of the simplified model reported in [14], where a LuGre-like dynamic model has been selected for the implementation of the friction [15], [16].

Due frictional effects, the passive tendon gives different contributions to the torques on joints 3 and 4, and the last line of matrix  $H_c$  of eq. (7) has to be split, as following:

$$H_{c2} = \begin{bmatrix} r_{11} & r_{21} & 0 & 0 \\ -r_{11} & r_{21} & 0 & 0 \\ 0 & 0 & r_{33} & 0 \\ 0 & -r_{24} & -r_{34} & -r_{44} \\ 0 & 0 & -r_{35} & 0 \\ 0 & 0 & 0 & r_{45} \end{bmatrix} \quad (10)$$

The relation between joint torques and tendon forces is then ruled by

$$\tau = H_{c2}^T f \quad (11)$$

where the total tendon force vector  $f$  (the vector of the forces actuated by the tendons on the mechanical structure) defined in (8), has been redefined as:

$$f = \begin{bmatrix} f_1 \\ f_2 \\ f_3 \\ f_4 \\ f_5^3 \\ f_5^4 \end{bmatrix} \equiv \begin{bmatrix} f_1^a - f_1^f \\ f_2^a - f_2^f \\ f_3^a - f_3^f \\ f_4^a - f_4^f \\ -K_t(\theta_3 r_{35} - p_5) \\ -K_t(p_5 - \theta_4 r_{45}) \end{bmatrix} \quad (12)$$

$$\ddot{p}_5 = (-f_5^f + f_5^3 - f_5^4)/m_5 \quad (13)$$

where  $f^f = [f_1^f \ f_2^f \ f_3^f \ f_4^f \ f_5^f]^T$  is the vector of the tendon friction forces,  $p_5$  and  $m_5$  are respectively the position and the mass of the passive tendon. The friction acting on the tendons is due to the curvature of the path and to the tendon tension and it depends on the friction coefficient and on the total curvature angle (see [10] for additional details). The assumptions  $f_i^f \equiv F^f$ ,  $f_i^s \equiv F^s$ , and  $\mu_i \equiv M$  are posed in the friction model (9) and  $v_t \equiv v$  is the tendon velocity. The variables  $f^n$  and  $\mu^d$  are defined as:

$$\hat{f}_i^n \hat{\mu}_i^d = f_i^n \mu_i^d \quad i \in \{1, \dots, 5\} \quad (14a)$$

$$\left. \begin{aligned} f_i^n &= |f_i^s| + |f_i^a| \\ \hat{f}_i^n &= |\hat{f}_i^s + \hat{f}_i^a| = f_i^n \alpha(\varphi_i) \end{aligned} \right\} \quad i \in \{1, \dots, 4\} \quad (14b)$$

$$\left. \begin{aligned} f_5^n &= |f_5^3| + |f_5^4| \\ \hat{f}_5^n &= |\hat{f}_5^3 + \hat{f}_5^4| = f_5^n \alpha(\varphi_5) \end{aligned} \right\} \quad (14c)$$

The angle  $\varphi_i$  is the  $i$ -th element of the curvature vector  $\varphi(\theta)$ , is computed as follows:

$$\varphi = \begin{bmatrix} 1 & 0 & 0 & 0 \\ 1 & 0 & 0 & 0 \\ 0 & 1 & 0 & 0 \\ 0 & 1 & 1 & 0 \\ 0 & 0 & 0 & 0 \end{bmatrix} |\theta| + \varphi^{\text{off}} \quad (15)$$

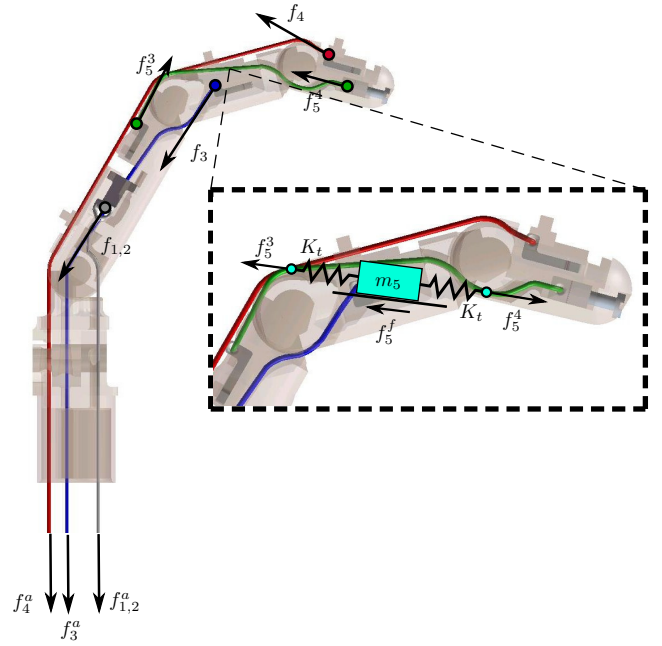


Fig. 4. Schematic representation of the forces applied by the tendons on the finger and detail of the passive tendon implementation.

where  $\varphi^{\text{off}}$  is the path curvature vector for  $\theta = 0$  (due to the tendon pathways geometry). In (14), the variables  $f_i^n$  and  $\mu_i^d$  are respectively used in place of the normal force  $F^n$  and the friction coefficient  $M^d$  in (9), where  $\alpha(\varphi_i)$  is the ratio between the arithmetic sum of the forces at the two ends of the tendon and the modulus of the normal force  $\hat{f}_i^n$  exerted by the tendon on the curved surface. The function  $\alpha(\varphi_i)$  has been introduced to take into account the dependence of the normal force  $\hat{f}_i^n$  from both the joint angles and the finger structure. Since the friction coefficient is multiplied by the normal force in order to obtain the friction level [16], a normalized friction coefficient  $\mu_i^d$  is used in place of  $\hat{\mu}_i^d$ , and  $f_i^n$  is used in place of  $\hat{f}_i^n$ , as in (9a); as reported in [13], [17] the friction coefficient  $\mu_i^d$  depends only on the total curvature angle  $\varphi_i$ :

$$\mu_i^d = \hat{\mu}_i^d \alpha(\varphi_i) = \frac{1 - e^{-\mu_e \varphi_i}}{1 + e^{-\mu_e \varphi_i}}, \quad i \in \{1, \dots, 5\} \quad (16)$$

where  $\mu_e$  is the Coulomb friction coefficient identified from experiments; in this system, has been considered  $\mu_e = 0.11$  (see [10] for further details).

### C. Joint Friction Model

The model (9) has been adopted also for simulating the joint friction. In this case,  $F^f$  is the torque loss  $\tau^f$  and the friction parameters  $M^d$  and  $M^c$  are suitable constants. The normal force  $F^n$  is the modulus of the reaction force  $R$  acting on a given joint, and  $v \equiv \dot{\theta}$  is the joint angular velocity. In case no external forces act on the finger,  $R$  depends on the forces applied by the tendons only and it

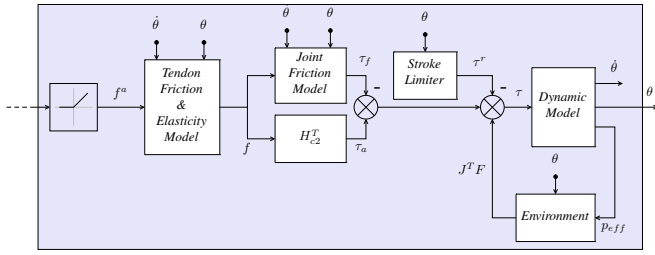


Fig. 5. Diagram of the finger model.

is given by:

$$\begin{aligned}
 R_1 &= |\vec{f}_1^t + \vec{f}_2^t + \vec{f}_3^t + \vec{f}_4^t| \\
 R_2 &= |\vec{f}_1^t + \vec{f}_2^t + \vec{f}_3^t + \vec{f}_4^t| \\
 R_3 &= |\vec{f}_3^t + \vec{f}_4^t + \vec{f}_5^a| \\
 R_4 &= |\vec{f}_4^t + \vec{f}_5^a|
 \end{aligned} \quad (17)$$

In case an external force is acting on the finger, the resultant must be added to the each joint. Hence, high values of  $R$ , and consequently of the frictional forces acting on joints, can be obtained by excessive internal or external forces.

#### D. Finger Dynamic Model

The classical Euler-Lagrange dynamic model is derived, as the finger is regarded as a four links robot:

$$M(\theta)\ddot{\theta} + C(\theta, \dot{\theta})\dot{\theta} + G(\theta) = H_{c2}f - \tau^f - \tau^r(\theta) + J^T F \quad (18)$$

where  $f$  is defined in (12) and then takes into account for the tendon forces and friction,  $M(\theta)$  and  $C(\theta, \dot{\theta})$  are the inertia matrix and the matrix of the Coriolis plus centrifugal terms respectively,  $G(\theta)$  is the gravitational matrix and  $\tau^r(\theta)$  is the reaction torque vector due to the joint stroke limiters.

#### V. FINGER SIMULATION AND CONTROL

The finger model has been implemented in the Matlab/Simulink simulation environment; in according with the sensory apparatus integrated into the finger, [7], the model measurable outputs are the joint angles  $\theta$  and the force vector  $f$  exerted by tendon on the finger structure. A schematic of the finger model is represented in Fig. 5, where are highlighted the tendon model, the joints friction model, the joints stroke limiter that enforces (2), the environment, and the dynamical model expressed by (18).

The control implemented is a simple proportional position control in the joint space; the desired joint torque  $\tau^d$  is computed as:

$$\tau^d = K_P(\theta^d - \theta) \quad (19)$$

In the generation of the joint reference trajectories  $\theta^d$  the constraint imposed by the passive tendon has been taken into account; so  $\theta_4^d$  depends on  $\theta_3^d$  as in the following:

$$\theta_4^d = \frac{1}{r_{45}} \left( r_{35} \theta_3^d + \frac{f_5^d}{K_t} \right) \quad (20)$$

where  $f_5^d$  is desired tension on the passive tendon.

In order to compute the actuation forces  $\hat{f}^a$  given the desired torques  $\tau^d$ , the pseudo-inverse  $H_c^{T+}$  of the coupling matrix is used:

$$f^m = H_c^{T+} \tau^d \quad (21a)$$

$$\hat{f}^a = f^m + \lambda f^k \quad (21b)$$

where  $f^m$  is the minimum module force vector so that  $\tau^d = H_c^T f^m$ ,  $f^k$  is a base of the null space of  $H_c^T$ , and  $\lambda \in \mathbb{R}$  is chosen in order to impose the tendon tensions above a certain threshold  $f^0$  (see [12] among others for further details):

$$\lambda = \max_{i \in \{1, \dots, 5\}} \frac{f_i^0 - f_i^m}{f_i^k} \quad (22)$$

The forces involved in (21) are five elements vectors; the input force of the tendon finger  $f^a$  is computed discarding the last force, related to the passive tendon:

$$f_i^a \equiv \hat{f}_i^a \quad i \in \{1, \dots, 4\}$$

Due to the force closure property and neglecting dynamic and friction forces, the desired tension on the passive tendon is univocally determined by the actuation forces  $f_i^a$ ; the computation of the desired passive tendon force is considered to ensure a minimum tension level  $f_0^5$  to the passive tendon.

In Fig. 6 the results of the simulation of the proposed finger model are reported. Fig. 6(a) shows the references angles: it can be observed that, even with this simple control strategy, a fairly low tracking error is obtained, as shown in Fig. 6(b). In the Fig. 6(c) the tension forces are shown: the dashed lines are the forces  $\hat{f}_i^a$  computed by the control, and the solid lines represent the five elements  $[f_1 \ f_2 \ f_3 \ f_4 \ f_5^A]$  of the vector  $f$  defined in (12), while the dotted line in the bottom plot is the fourth element  $f_4^3$  of  $f$ .

#### VI. CONCLUSIONS

In the process of engineering a functional robotic hand, an accurate modeling is fundamental step both as feedback for the design process and as starting point to design and tune the control system. Employing a combination of information extracted by experiments, CAD drawings, and past experiences, a model for a bio-inspired finger has been realized and described. The more interesting points emerging from this model are centered on how friction on joints and tendons behaves in different condition, and which implications brings the use of a passive tendon that couples the distal and median joints. We highlight the following points:

- Tendon friction coefficient is a function of joints angles, so any control strategy, as the one described in [10], must consider it.
- Joint friction coefficient depends on the sum of the tendon forces, as expressed by (17). High forces or friction coefficient can cause a grip on a phalanx; this can also happen if reference torques are too high. By these consideration emerges that reducing friction is an obvious advantage, but joint friction is more crucial than tendon friction; moreover control strategies must consider that excessive tendon tensions have to be avoided.

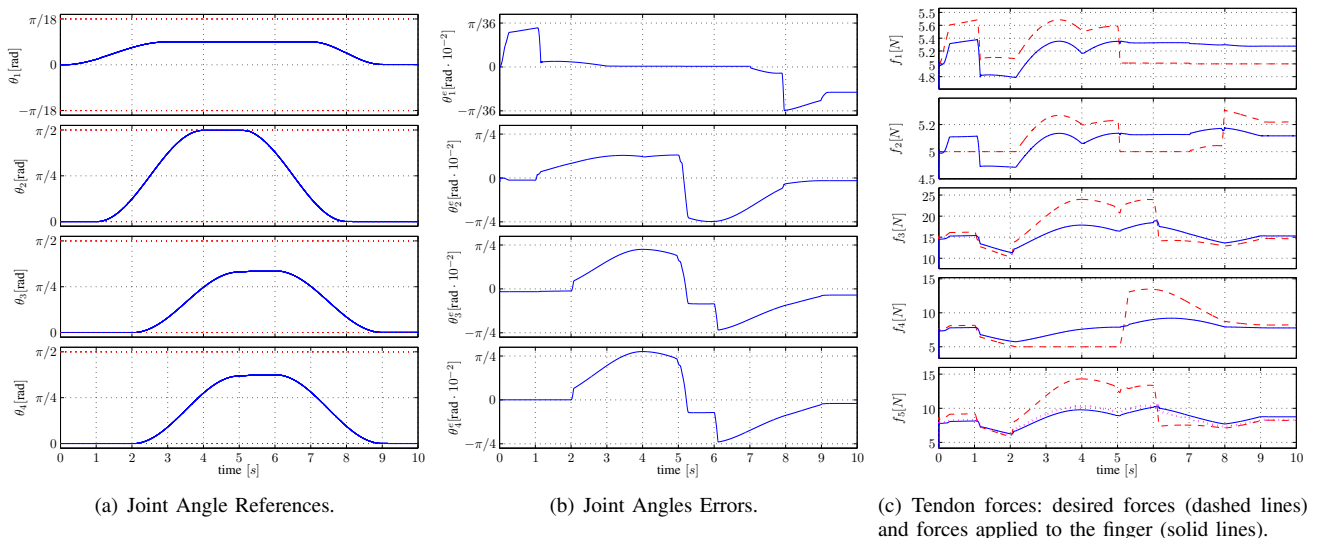


Fig. 6. Torques and forces, before and after tendons or joints friction losses

- Thanks to the tendon network property of force closure, it is possible to (approximately) control the force on the passive tendon by acting on other tendon forces. This assumption is verified when the finger inertial forces are small, and the friction on the whole tendon network is not preponderant (or control compensated).

From these consideration, control strategies will be purposely designed, and firstly tested on the described model, that will be enriched by actuator models and complex contact scenario.

#### REFERENCES

- [1] A. Bicchi, "Hands for dextrous manipulation and robust grasping: a difficult road towards simplicity," *IEEE Trans. on Robotics and Automation*, vol. 16, no. 6, pp. 652–662, December 2000.
- [2] F. Lotti, P. Tiezzi, G. Vassura, L. Biagiotti, G. Palli, and C. Melchiorri, "Development of UB Hand 3: Early results," in *Proc. IEEE Int. Conf. on Robotics and Automation*, 2005, pp. 4488–4493.
- [3] C. Lovchik and M. Diftler, "The robonaut hand: a dexterous robot hand for space," in *Proc. IEEE Int. Conf. on Robotics and Automation*, 1999.
- [4] A. Deshpande, J. Ko, D. Fox, and Y. Matsuoka, "Anatomically correct testbed hand control: Muscle and joint control strategies," in *Proc. IEEE Int. Conf. on Robotics and Automation*, 2009, pp. 4416–4422.
- [5] L. Birglen, T. Lalibert, and C. M. Gosselin, *Underactuated Robotic Hands, Chap. 2*. Springer Berlin / Heidelberg, 2008.
- [6] D. D. Wilkinson, M. V. Weghe, and Y. Matsuoka, "An extensor mechanism for an anatomical robotic hand," in *Proc. IEEE Int. Conf. on Robotics and Automation*, 2003.
- [7] G. Berselli, G. Borghesan, M. Brandi, C. Melchiorri, C. Natale, G. Palli, S. Pirozzi, and G. Vassura, "Integrated mechatronic design for a new generation of robotic hands," in *Proc. of the IFAC Symposium on Robot Control*, Gifu, Japan, 2009.
- [8] H. Liu, P. Meusel, G. Hirzinger, M. Jin, Y. Liu, and Z. Xie, "The modular multisensory DLR-HIT-Hand: Hardware and software architecture," *IEEE/ASME Transactions on Mechatronics*, vol. 13, no. 4, pp. 461–469, 2008.
- [9] C. Melchiorri and M. Kaneko, *Springer Handbook of Robotics, Chap. 15, Robot Hands*, B. Siciliano and O. Khatib, Eds. Springer, 2008.
- [10] G. Palli, G. Borghesan, and C. Melchiorri, "Tendon-based transmission systems for robotic devices: Models and control algorithms," in *Proc. IEEE Int. Conf. on Robotics and Automation*, 2009.
- [11] L. Sciavicco and B. Siciliano, *Modeling and Control of Robot Manipulators*. McGraw-Hill, 1996.
- [12] R. M. Murray, Z. Li, and S. S. Sastry, *A mathematical introduction to robotic manipulation, Chap. 6, Hand Dynamics and Control*. CRC Press, 1994.
- [13] G. Palli and C. Melchiorri, "Model and control of tendon-sheath transmission system," in *Proc. IEEE Int. Conf. on Robotics and Automation*, 2006.
- [14] —, "Optimal control of tendon-sheath transmission systems," in *Proc. of the IFAC Symposium on Robot Control*, 2006.
- [15] C. C. de Wit, H. Olsson, K. J. Åström, and P. Lischinsky, "A new model for control of systems with friction," *IEEE Transactions on Automatic Control*, vol. 40, pp. 419–425, 1995.
- [16] H. Olsson, K. J. Åström, C. C. de Wit, M. Gäfvert, and P. Lischinsky, "Friction models and friction compensation," *European Journal of Control*, vol. 3, pp. 176–195, 1998.
- [17] M. Kaneko, T. Yamashita, and K. Tanie, "Basic considerations on transmission characteristics for tendon drive robots," in *Advanced Robotics, 1991. 'Robots in Unstructured Environments', 91 ICAR., Fifth International Conference on*, 1991, pp. Page(s):827 – 832 vol.1.